Materials Science-Poland, 41(1), 2023, pp. 161-176
http://www.materialsscience.pwr.wroc.pl/
DOI: 10.2478/msp-2023-0012

sciendo

Comparative evaluation of mechanical properties of short aramid fiber on thermoplastic polymers

Ali Arı[1,*], Ali Bayram[2], Mehmet Karahan[3], Orhun Arslan[4]

[1]Department of Weapon Industry Technician, Vocational School of Higher Education, Ostim Technical University, Ankara, Turkey; ORCID: https://orcid.org/0000-0003-2702-2982

[2]Department of Mechanical Engineering, Bursa Uludag University, Bursa, Turkey; ORCID: https://orcid.org/0000-0001-7311-8358

[3]Department of Textile, Vocational School of Higher Education Bursa Uludag University, Bursa, Turkey; ORCID: https://orcid.org/0000-0003-3915-5598

[4]Kırpart Automotive Side Industry and Trade Inc., 16800, Bursa, Turkey; ORCID: https://orcid.org/0000-0001-5918-0980

This study investigated the mechanical performance of short aramid fiber on polypropylene, polyethylene, polyamide 6, and polyamide 12. Extrusion, press molding, and CNC cutting methods were used in the production of composite samples. Tensile, three-point bending, drop weight and hardness tests of the composites were carried out. As the fiber volume fractions increased, the mechanical properties of the composites improved, but the most efficient fiber fractions for each matrix changed. To analyze the performance of the fibers in the matrix on the composites, scanning electron microscope (SEM) images of the fractured surfaces as a result of tensile and drop weight tests were examined. As the fiber volume fractions increased, the fiber deformation increased, and as a result, the mechanical performance of the composites was adversely affected. Analysis of variance (ANOVA) and F test were performed using signal/noise values to analyze in detail the effect of experimental parameters on output values. Finally, the results of a regression equation model were compared with the experimental readings. It was found to be in good agreement with the model and the results of the experiment.

Keywords: *aramid fiber, polymer-matrix composites, mechanical properties, ANOVA, regression*

1. Introduction

Composites consist of a continuous phase (matrix) and inclusions of dispersed fibers. The fibers provide the strength of the material, while the matrix helps maintain the shape of the part. The matrix-fiber interface is crucial for transferring the load from the matrix to the fiber [1]. Composites, considered advanced engineering materials, are used in various industries such as aerospace, defense, construction, and automotive [2]. Thanks to the fibers, the properties of composite materials such as rigidity, high strength, and fracture toughness improve [3].

Aramid fibers have excellent impact resistance and are widely used in bulletproof vests, armored tanks, and other military applications [4]. Compared to the properties of inorganic reinforcing fibers such as glass and carbon fibers, aramid fibers have high hardness, strength, and low density, which provide a significant advantage [5]. Aramid fibers have low layer thickness and high flexibility compared to alternative fibers. Basically, they are widely used in applications such as ballistic applications, helicopter propellers, and outdoor materials [6]. Shortfiber-reinforced composites are commonly used in the automobile and defense industry because of their low production cost, high production speed, high strength, hardness, and impact resistance [7].

Chopped aramid fiber is preferred as a reinforcement element to the rubber matrix because of its high modulus of elasticity and fatigue and superior thermal and corrosion performance [8]. Gao et al. analyzed the mechanical properties of chopped

* E-mail: ali.ari@ostimteknik.edu.tr

aramid-fiber-reinforced rubber composites (AFRC) by numerical and experimental methods [9]. A finite element model was developed for the estimation of the mechanical properties of the experimental data. Arroyo and Bell analyzed the mechanical behavior of short aramid-fiber-reinforced polypropylene and ethylene-propylene-diene composites. They concluded that the most optimal design is 20% aramid-fiber-reinforced polypropylene [10].

Similarly, Sarasini et al. observed that the hybrid effect of aramid and basalt fibers positively affects the impact properties [11]. Shibulal and Naskar investigated the effect of two structurally different short aramid fibers (Technora and Twaron) on thermoplastic polyurethane's mechanical and thermal properties [12]. Young's modulus of Technora-polyurethane was three times higher than that of Twaron-polyurethane. In addition, a brittle fracture was observed in both composites during the tensile test [13]. Bazan et al. produced biocomposite samples using biobased polyamide and two different types of fibers (aramid and basalt). They found that the reinforcement of the fibers increased the hardness and strength properties and caused an increase in the dissipation of mechanical energy. The addition of 10% short aramid fiber increased the tensile strength by about 15% [14]. In another study, the mechanical properties of polyurethane composites were reinforced with two types of short aramid fibers, m-aramid (Teijin-Conex) and copoly(p-aramid) (Technora), were investigated. Although both fibers did not have any surface treatment, it effectively increased the mechanical properties of polyurethane [15].

The focus of this article is to analyze in detail the mechanical effect of chopped (short) aramid fiber (AF) on polypropylene (PP), polyethylene (PE), polyamide 6 (PA6), and polyamide 12 (PA12) matrix composites. In this context, statistical analysis was performed to analyze the parameters affecting the results of the tests. Finally, a regression equation model was developed based on experimental data.

2. Materials and methods

2.1. Material and production method

In experimental studies, PP, PE, PA6, and PA12 were used as matrix materials, and aramid (Twaron) fibers were used as reinforcement materials. 6-mm length chopped fiber was used in the composites. Fiber volume fractions were determined as 10%, 20%, and 30%. Mechanical properties of matrix and fiber material were taken from catalog values (Table 1). Preparation of test samples and all related tests were carried out in Bursa Technology Coordination and R&D Center (Bursa, Turkey).

Siva et al. used extrusion and injection methods to prepare poly(lactic acid) (PLA) matrix composites. The mechanical performance of the samples prepared using the extrusion method was 17% better than those prepared by injection. The twin screw extruder's high-intensity mixing results in a decrease in the composite material's void content [16].

Therefore, in our study, a twin-screw extruder (Polmak Plastik 22-mm Lab type research extruder) was used to produce composites. The temperature for the five zones in the extruder were determined using the literature and the product catalog of the materials (195°C–215°C–225°C–225°C–240°C and 30 rpm for PP; 170°C–195°C–220°C–220°C–230°C for PE and 30 rpm; 240°C–240°C–250°C–260°C–285°C for PA6 and 30 rpm; 190°C–200°C–210°C–220°C–230°C for PA12 and 30 rpm) [17, 18]. Afterward, the composites coming out of the extruder as filaments were then granulated with a cutter. These granules were converted

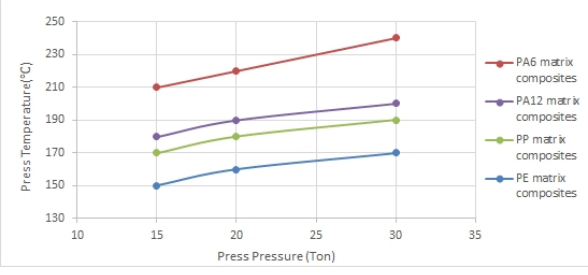

Fig. 1. Press molding production parameters

Table 1. Mechanical properties of materials

Materials	Density (kg/m^3)	Tensile Strength (MPa)	Elastic Modulus (GPa)	Types	Producers
PP	0.9	38	1.2	EH251	Petkim
PE	0.95	24	1	High density, B00552	Petkim
PA6	1.13	85	2	F223-D	Akulon
PA12	1.02	60	1.5	AMN Black T6LD	Arkema Rilsamid
AF	1.44	2800	60	Short-cut fiber	Twaron

into composite plates with 500 mm × 500 mm dimensions by the press molding method. The press molding process was carried out in three stages, as shown in Figure 1. It was held for 120 s in the first stage, 180 s in the second stage, and 60 s in the third stage, and 4-mm thick plates were formed. The test samples were prepared by cutting the relevant plates into standard sizes with a CNC machine.

2.2. Mechanical testing

This section conducted tensile, bending, drop weight, and shore D hardness tests. Five specimens were prepared and tested for each test. The tensile test was carried out on the Besmak-BMT 100E brand Universal tensile tester. The samples for the tensile test were prepared according to TS EN ISO 527-2 type 2 standards. The tensile speed was set to 2 mm/min, and the pre-stress value was set to 10 N. The tests were carried out at a temperature of 21°C. The fractured surfaces of the samples with 30 vol% aramid fiber content as a result of the tensile test were examined with a Hitachi TM3000 brand scanning electron microscope (SEM).

According to the Kelly-Tyson model (Equation 1) and the tensile test results, the fiber performance of aramid fiber on matrix materials was calculated [19, 20].

$$\sigma_c = \lambda_f \sigma_f V_f + \sigma_m (1 - V_f) \tag{1}$$

where σ_c, σ_f, and σ_m are the tensile strengths of the composite (Figure 2), reinforcement, and matrix, respectively (Table 1). V_f is the fiber volume content of the composite, and λ_f is the fiber efficiency factor.

Flexural strength refers to the maximum stress a material can withstand before it fails or breaks when subjected to a bending or flexing force. The three-point bending test was performed on a Shimadzu brand tester. Five tests were performed for each parameter. Test samples were prepared according to TS EN ISO 178-3 standards. The distance between the supports is 64 mm, the test speed is 2 mm/min, and the test ambient temperature is 21°C.

The sudden applied load a specimen can absorb before breaking is called impact strength. The usage of natural fiber-reinforced composites is relatively low because of the reduced mechanical properties and because their use significantly impacts strength. Drop-weight tests were performed in Instron/Ceast 9340 impact tester. The samples were prepared for drop-weight impact tests according to TS EN ISO 6603 standards. Also, the ambient temperature was adjusted to 21°C. Fractured surface images of 30 vol% aramid fiber content samples were inspected with Hitachi TM3000 SEM.

The hardness of the composites was measured according to the shore D scale. For the tests, a Hildebrand hardness-measuring device was used. The hardness test samples were prepared according to TS EN ISO 868 standards, and the ambient temperature was set to 21°C.

2.3. Experimental design and ANOVA analysis

In our study, it is necessary to determine the experimental factors and levels to interpret the input variables' effect on the output values. The experimental design matrix (Table 3) was created by changing the parameters specified in Table 2 [21].

Signal value (S) represents the actual value given by the system and is intended to be measured. The noise factor (N) represents the share of unde-

Table 2. Experiment factors and levels

Factors	1. Level	2. Level	3. Level	4. Level
A- Matrix Type	PP	PE	PA6	PA12
B- Fiber volume fraction %	0*	10	20	30

*None and 0 represent the same levels

Table 3. Experimental design

Experiment No.	**A-Matrix Type**	**B-Fiber volume fraction %**
1	1	1
2	2	1
3	3	1
4	4	1
5	1	2
6	1	3
7	1	4
8	2	2
9	2	3
10	2	4
11	3	2
12	3	3
13	3	4
14	4	2
15	4	3
16	4	4

sired factors in the measured value. According to this approach, the following equation (2) is used to calculate the S/N ratio [22].

$$\frac{S}{N} = -10\log_{10}\left[\frac{1}{n}\sum_{i=1}^{n}\frac{1}{y_i^2}\right] \tag{2}$$

where y is the measurement value, and n is the number of experiments.

The analysis of variance reveals how much the factors investigated influence the output value used to gauge the quality and what effects different levels have. Furthermore, the statistical reliability of the results obtained was examined. For this purpose, firstly, the SS_T value (sum of total squares), which represents the overall variability of the signal/noise (S/N) ratio, is calculated according to equation (3) [23].

$$SS_T = \sum_{i=1}^{n}(\eta_i - \eta_m)^2 \tag{3}$$

where η_i is the signal-to-noise ratio calculated over the measured value, η_m is the average of the calculated signal-to-noise ratios over the measured value, and n is the total number of experiments [24]. The SS_T value is the sum of the squares of the two factors of SS_A (sum of squares of factor A) and SS_B (sum of squares of factor B), and the SS_E value is the sum of the squares of the margin of error. The sum of each factor's squares was calculated separately using equation (4).

$$SS_j = \sum_{i=1}^{k_j}\left[n_{ji}x(\eta_{ji} - \eta_m)^2\right], \quad j = A \text{ or } B \tag{4}$$

where k_j represents the number of levels of the A or B factor, n_{ji} is the number of experiments at the i level of the A or B factor, η_{ji} the S/N ratio of the A or B factor at the i level, and η_m the average S/N ratio [24].

For the next step, the F-Test is performed by calculating equation (5) to present how much each experimental factor affects the test results.

$$F = \frac{\frac{SS_j}{\mathbf{k}-1}}{\frac{SS_E}{\mathcal{N}-k}} \tag{5}$$

where **k**-1 is the degree of freedom numerator by subtracting one from the number of groups, $\mathcal{N} - k$ is the degree of freedom for the denominator, which is determined by, $\mathcal{N}$ subtracting the number of groups from the number of observations in all groups [25].

3. Results and discussion

3.1. Tensile properties and fractography

It was observed (Figure 2) that the tensile strength of all composite materials increased as the fiber volume fraction increased, so the highest values for tensile strength were obtained at the 30 vol% level of fiber fraction reinforcement materials.

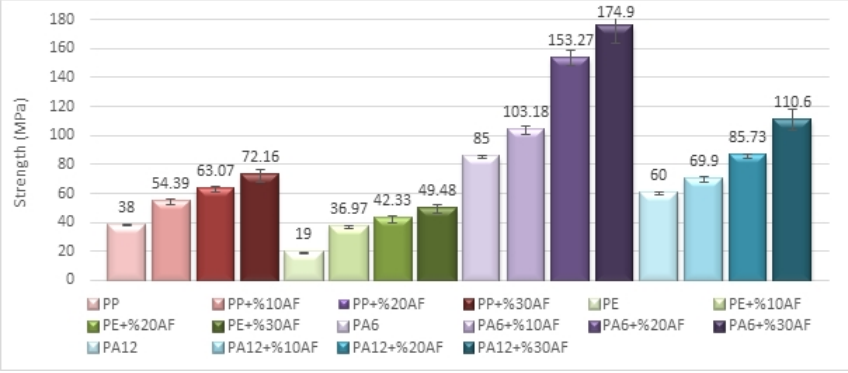

Fig. 2. Tensile test results of composites

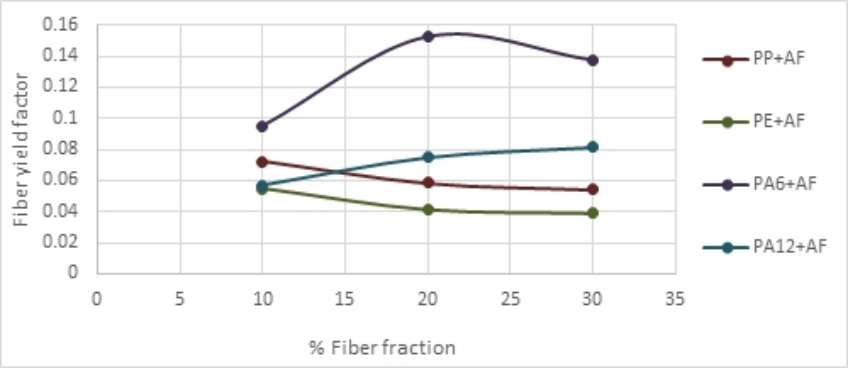

Fig. 3. Fiber efficiency factor in composites

The following is a summary of the test results: (1) It was observed that the highest enhancement for each composite was obtained for 30 vol% reinforcement cases; 1 (2) 30 vol% AF increased the tensile strength of PP 2.4 times and increased it from 38 MPa to 72.2 MPa; (3) 30 vol% AF increased the tensile strength of PE 2.6 times and increased it from 19 MPa to 49.5 MPa; (4) 30 vol% AF increased the tensile strength of PA6 1.9 times and increased it from 85 MPa to 175 MPa, (5) 30 vol% AF increased the tensile strength of PA12 1.85 times and increased it from 60 MPa to 110.1 MPa. The increase in tensile strength is approximately linear with the increase in fiber content, and for all composites, the increase in strength is approximately twice that at 30% AF content.

When the results of the tensile tests were examined, it was seen that the fiber fraction directly contributed to the mechanical properties of the composite. With the increase in fiber fraction, however, the effect of fiber on the composite decreased (Figure 3). It was observed that the deformation between matrix and fiber increased with increasing fiber fraction [26].

According to the results of the tensile tests, the performance of aramid fiber on four matrices was examined, and the highest performance was seen in the composites made with PP and PE. It increased PP 2.1 times and PE 2.6 times. The basis of a good matrix and fiber compatibility is the creation of a good interface [27]. This means that the surface energy of the matrix material should be low, and the surface energy of the fiber should be high [28]. Molecules in a low-surface-energy liquid are not strongly attracted to each other; instead, they tend to spread and adhere to the surface, so a high-free-energy liquid will not bind to the fiber surface [29]. To form a good bond, the matrix surface energy must be low [30]. Because the surface energy of the PE and PP matrix is lower than the

other matrices [31, 32], the PE and PP matrix composites performed better than the others. Likewise, because the surface energies of PA6 and PA12 are close, the performance of aramid fiber on these matrices is almost equal. The surface energy properties of polymers and aramid fiber are given in Table 4. These values differ slightly in the literature, but the surface energy order is the same in all of them. The lowest values are for PP and PE, then the next higher is for PA12, and the highest is for PA6.

Table 4. Surface energies of polymers and aramid fiber

Materials	Surface Energy (mN/m)	References
PP	30–31	[33–36]
PE	30–31	[33–36]
PA6	38	[33, 35]
PA12	36	[33, 35, 36]
AF	51	[37, 38]

When the fiber efficiency factor-fiber fraction curve indicated in Figure 3 is examined, the fiber efficiency varied with the increase in the fiber fraction. Fu et al. examined the effect of 8%, 16%, and 25% fiber (by weight) on the PP matrix. As the fiber fraction increased, the tensile strength of the composite decreased. They explained it as follows: As the fiber fraction increases, the fiber-fiber interaction in the extruder increases during the composite production. As a result, it has been stated that local deformations occur in the fiber and matrix. As a result, they concluded that the effect of the fiber on the matrix was reduced [19]. The same result is valid in our study. Especially when looking at PP and PE matrices, the fiber efficiency performance decreased as the fiber fraction increased. Figure 4 shows surface SEM images of samples reinforced with 30 vol.% AF. When these images were examined, local deformations were observed in PP + 30 vol% AF and PE + 30 vol% AF samples. However, it was observed that this situation was slightly different in PA12. In PA12, the yield of the fiber evolved into a horizontal line at 20–30% AF contribution. This shows us that the ideal fiber fraction for PA12 is 20–30% by volume AF. The perfect fiber fraction for PA6 is 20 vol% AF, and when this fiber fraction is exceeded, fiber efficiency decreases. In addition, this change in fiber yield is also due to the non-homogeneous distribution of the fiber in the matrix [39]. Wang et al. (2008) investigated the effect of fiber distribution on the mechanical properties of carbon fiber reinforced composites (CFRC) samples and concluded that the inhomogeneity of fiber distribution negatively affects the strength of composites. One reason for the decrease in fiber yield in AF-reinforced PP and PE is interpreted as the deterioration of homogeneity as this fiber content increases [40].

Figure 5 shows the SEM images of the fractured surfaces as a result of the tensile test of 30 vol% AF-reinforced composites. When SEM micrographs were examined, it was determined that the damage mechanism in composite materials occurred in three stages. It was observed that (1) microcracks formed in the matrix, (2) separation between the fiber and the matrix, and (3) separation at the interface and breaking of the fibers caused damage [41].

For a good quality adhesion between the fiber and the matrix to occur, the matrix must be able to wet the fiber well [42]. This means that the matrix will completely cover the rough surface of the fiber and will absorb all the air. Pull-out damage will occur in the composites if there is no good wetting between the matrix and the fiber [29]. When Figure 5 is examined, the damage mechanisms in the composite material are explained as follows: (1) It is seen that there is a pull-out in the fibers in places. This is due to the lack of a good quality adhesion between the fiber and the matrix. As a result, it means that in these parts, the fiber cannot adequately bear the load. (2) Dark circles around the fibers indicate local deformations. (3) It has been observed that with the increase of fiber content, bending and crossing occur in the fibers. This has negatively affected fiber performance. (4) As mentioned above, with the increase of fiber fraction, fiber-fiber interaction in the extruder increases, and local deformations occur in the fibers. As seen in the SEM images, the fibers were damaged. Therefore, fiber performance has decreased [43].

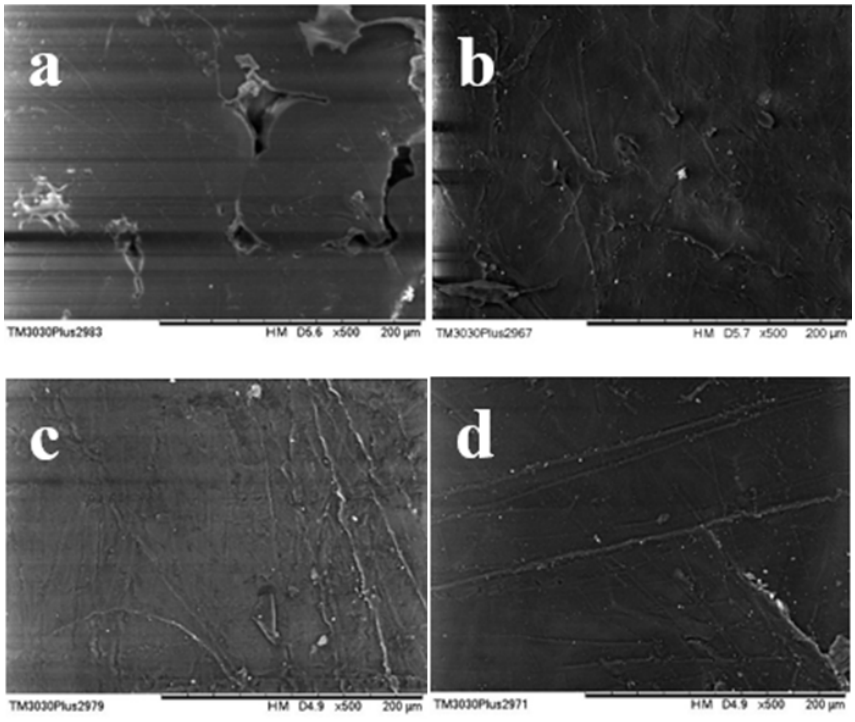

Fig. 4. SEM images of 30 vol% AF reinforced composite surfaces: (a) PP matrix, (b) PE matrix, (c) PA6 matrix, (d) PA12 matrix

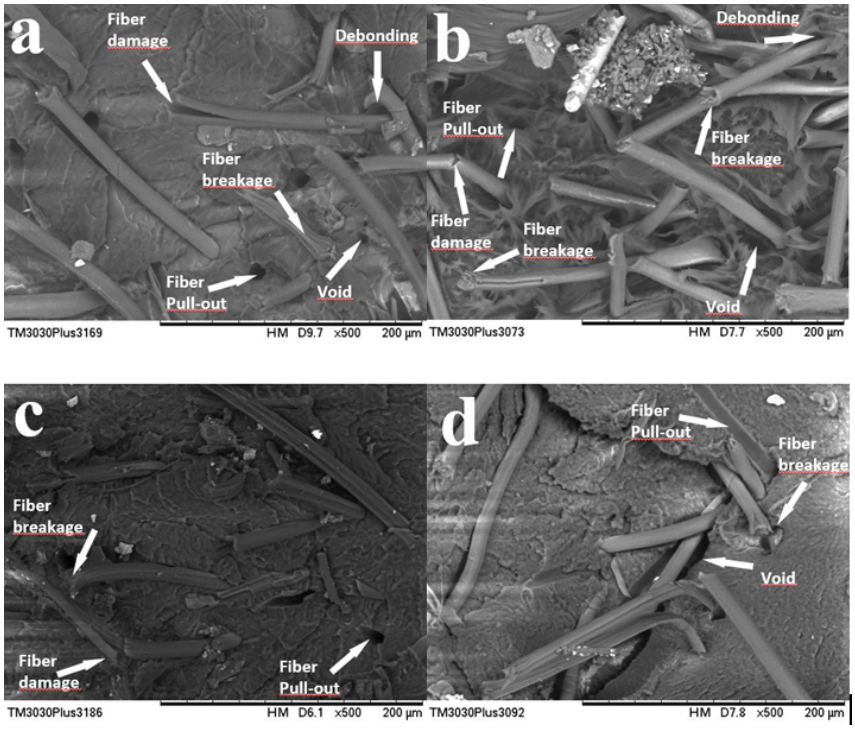

Fig. 5. SEM images of fractured surfaces of 30 vol% AF-reinforced composites (a) PP matrix, (b) PE matrix, (c) PA6 matrix, (d) PA12 matrix

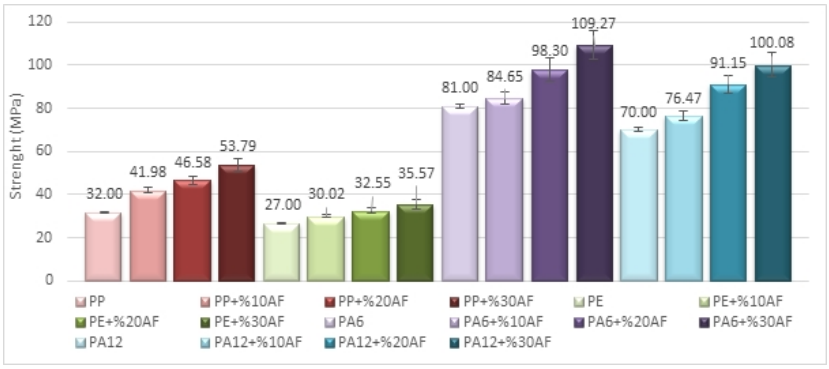

Fig. 6. Three-point bending test results of the composites

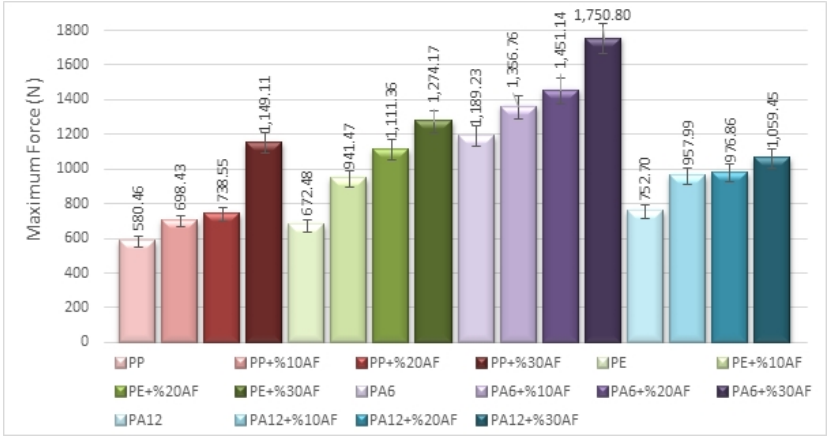

Fig. 7. Drop weight impact test results of the composites

3.2. Three-point bending properties

Figure 6 shows the results of the three-point bending test. It was observed that the bending stress values of PA6 matrix composites with high strength values are higher than PP, PE, and PA12 matrix composites with low strength values. In addition, as the fiber fraction increased, the bending stress increased [44, 45].

The following is a summary of the test results: (1) It was observed that the highest enhancement for each composite was obtained for 30 vol% AF reinforcement cases, (2) 30 vol% AF reinforcement increased the flexural strength of PP approximately 1.7 times by enhancing it from 32 MPa to 53.8 MPa, (3) 30 vol% AF reinforcement increased the flexural strength of PE 1.3 times by enhancing it from 27 MPa to 35.57 MPa, (4) 30 vol% AF reinforcement increased the flexural strength of PA6 1.4 times by enhancing it from 81 MPa to 110 MPa and (5) 30 vol% AF reinforcement the flexural strength of PA12 1.4 times by enhancing it from 70 MPa to 100 MPa.

3.3. Drop weight properties and fractography

The test results are shown in Figure 7, and it was observed that the force (based on the highest contacting forces) increased as the increasing fiber ratios increased.

The following is a summary of the test results: (1) It was observed that the highest enhancement for each composite was obtained for 30 vol% AF reinforcement cases; (2) 30 vol% AF reinforcement increased the impact resistance of PP approximately two times by enhancing it from 581 N to 1149 N; (3) 30 vol% AF reinforcement increased

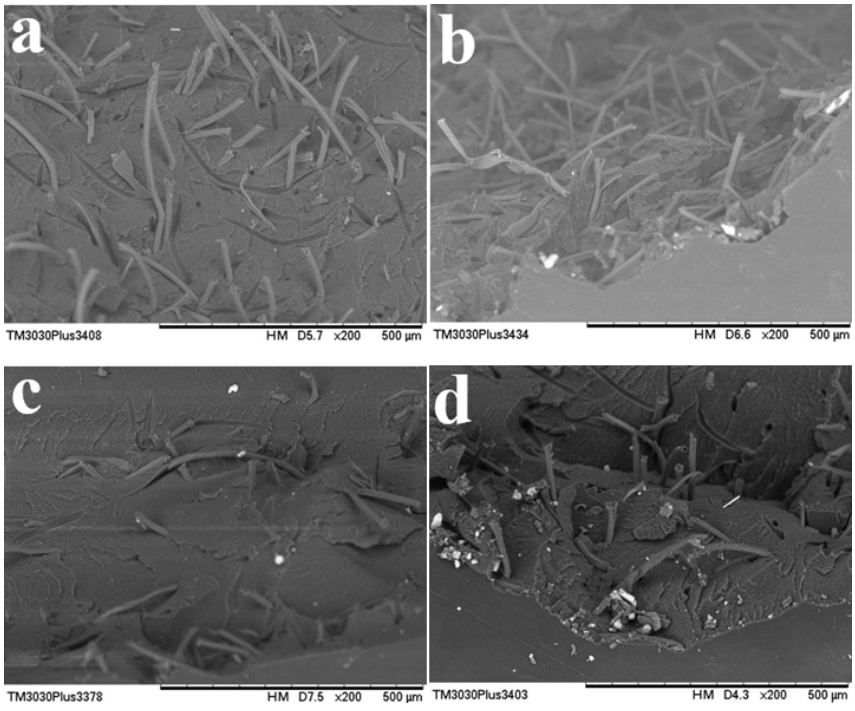

Fig. 8. SEM images of fractured surfaces of 30% AF reinforced composites (a) PP matrix, (b) PE matrix, (c) PA6 matrix, (d) PA12 matrix

the impact resistance of PE 1.9 times by enhancing it from 698 N to 1274 N; (4) 30 vol% AF reinforcement increased the impact resistance of PA6 1.5 times by enhancing it from 1189 N to 1750 N; and (5) 30 vol% AF reinforcement increased the impact resistance of PA12 1.4 times by enhancing it from 752.7 N to 1059 N.

When the test results were examined, aramid fiber showed the highest effect on the PP matrix. When we look at the other test results, the main reason for this high fiber-matrix compatibility of PE is that the surface energy of the PE matrix is lower than other polymer matrices.

In Figure 8, SEM images of fracture surfaces as a result of the drop weight test of 30 vol% AF-reinforced composites are given. All fibers were found to break brittle. The response of composite materials to impact is very complex. Under impact loading, the impactor has invisible or poorly detectable damage modes. Low-velocity impacts may not cause visible damage. Impact damages caused by the impact of composites are matrix cracking, delamination, and fiber damage. The damage, which starts with matrix cracking in low-speed impacts, causes delamination, and the fiber damage occurred because of the impact energy applied to the composite and continued to increase. It was observed that the impactor stuck in the sample and pierced the sample [46].

Pull-out is seen in composites. When the surface of the fibers is examined, it is seen that the surface is not covered with polymeric matrix, and the surface is clean. This indicates poor interfacial adhesion between the fiber and the matrix. Dark circles around the fibers indicate local deformation in the matrix around the fibers.

When the fracture surface of 30 vol% AF-reinforced composites in Figure 8 (ABC) was examined, it was seen that the fibers were clean. This showed that the fiber-matrix interface adhesion performance was not good.

When the fracture surfaces of the 30 vol%, AF-reinforced PA12 composites in Figure 8 (d) were examined, bending and crossing were observed in the fibers with increased fiber content. This adversely affected fiber performance [47].

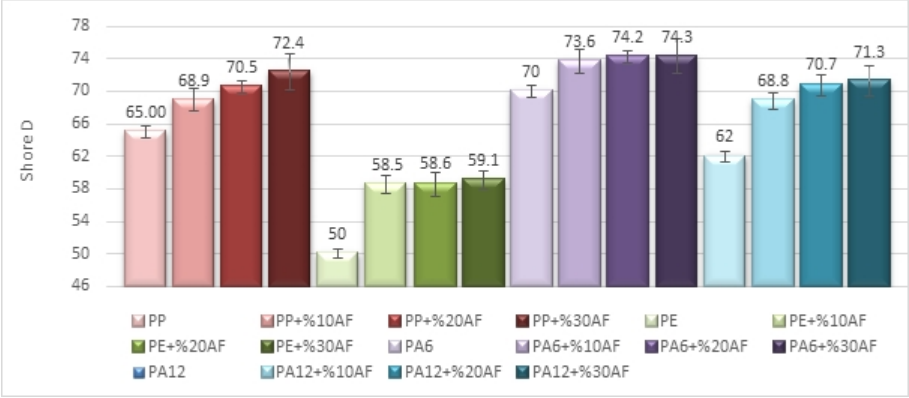

Fig. 9. Hardness test results of the composites

Table 5. S/N ratios of experimental results

Experiment No	Tensile strength (MPa)	S/N	Flexural strength (MPa)	S/N	Maximum force in drop weight (N)	S/N	Hardness Shore D	S/N
1	38	31.60	32	30.10	580.46	55.28	65	36.26
2	19	25.58	27	28.63	672.48	56.55	50	33.98
3	85	38.59	81	38.17	1189.23	61.51	70	36.90
4	60	35.56	70	36.90	752.70	57.53	62	35.85
5	54.39	34.71	41.98	32.46	698.43	56.88	69	36.76
6	63.07	36.00	46.58	33.36	738.55	57.37	71	36.96
7	72.16	37.17	53.79	34.61	1149.10	61.21	72	37.19
8	36.97	31.36	30.02	29.55	941.47	59.48	59	35.34
9	42.33	32.53	32.55	30.25	1111.40	60.92	59	35.36
10	49.48	33.89	35.57	31.02	1274.20	62.10	59	35.43
11	103.18	40.27	84.65	38.55	1356.80	62.65	74	37.34
12	153.27	43.71	98.3	39.85	1451.10	63.23	74	37.41
13	174.90	44.86	109.3	40.77	1750.80	64.86	74	37.42
14	69.90	36.89	76.47	37.67	957.99	59.63	69	36.75
15	85.73	38.66	91.15	39.20	976.86	59.80	71	36.99
16	110.60	40.88	100.1	40.01	1059.40	60.50	71	37.06

The following is a summary of the test results: (1) when the SEM images of the fracture of 30 vol% fiber-reinforced composites were examined, it was seen that there was a brittle fracture in the fibers; (2) it was observed that the impactor stuck in the sample and pierced the sample; (3) pull-out was observed in composites; (4) it was observed from the surface of the fibers that the surface was not covered with polymeric matrix, and the surface was clean, which indicated poor interfacial adhesion between the fiber and the matrix; (5) dark circles around the fibers indicate local deformation in the matrix around the fibers [48].

3.4. Hardness properties

The hardness test results are given in Figure 9. It was seen that the hardness values of the composites increased by the increment of fiber volume fraction, and the highest hardness value was obtained in aramid-fiber-reinforced PA6. This increment in the hardness of the composites can be explained as when the pressure is applied to the material, resistance occurs by the pressing matrix and fiber together. Because of this behavior, bonding happens between the fiber and the matrix, transfers the load to the interface more effectively, and strengthens

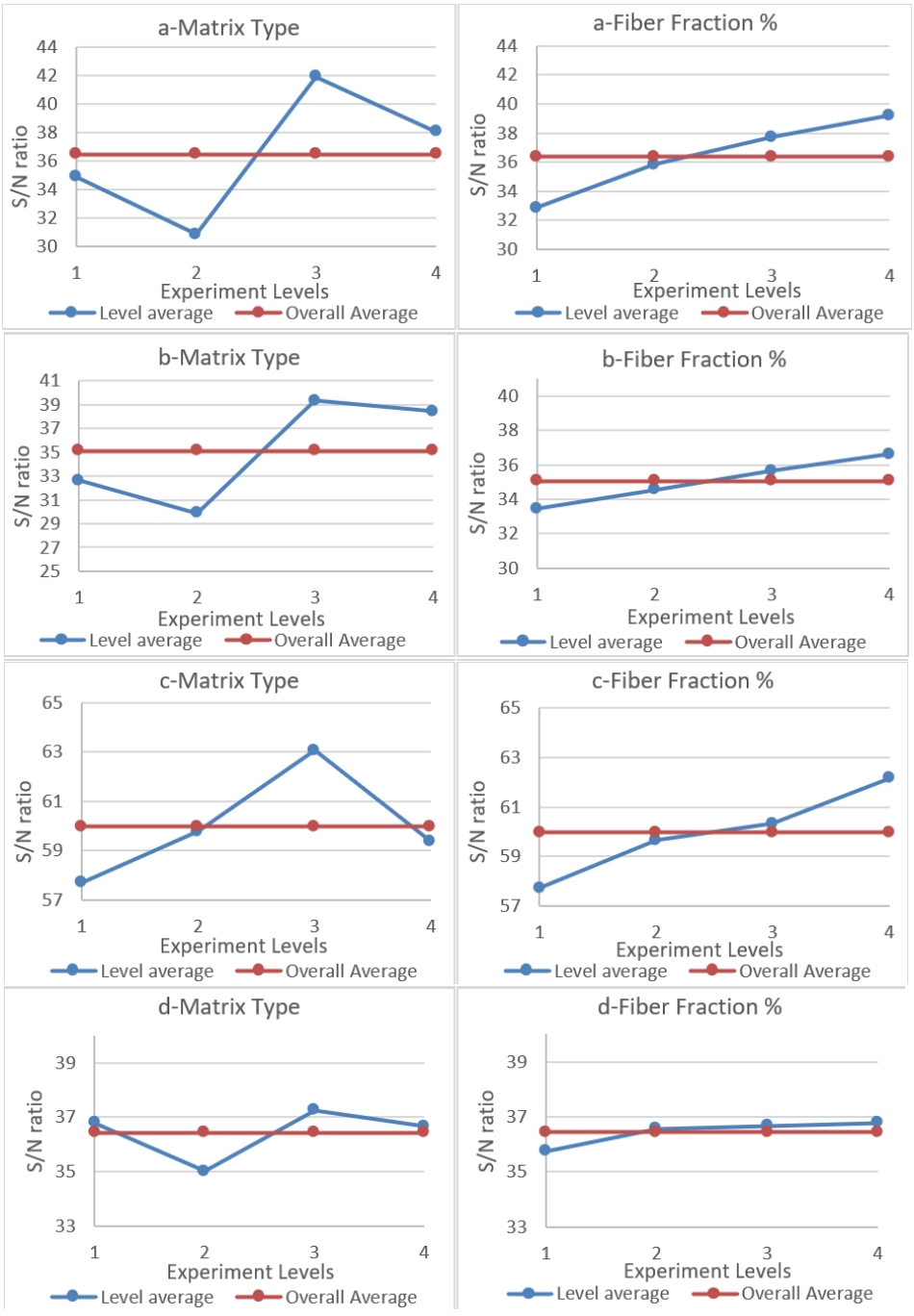

Fig. 10. (a) S/N ratios for tensile strength, (b) S/N ratio for flexural strength, (c) S/N ratio for dropped weight, (d) S/N ratio for hardness-shore D

the stiffness of the composite [49, 50]. With the fiber content growing, the number of attachment points increases, and the skeleton structure, as a whole, develops the material's ability to resist external pressure by inhibiting the movement of the composite [51, 52]. Impact of AF on hardness is significant only up to 10% of AF content, then it is negligible, especially for PE and PA.

Table 6. Results of ANOVA

For Tensile Test **S/N ratio: 35.75**		**Average S/N Values**							
	Degrees of Freedom	**Level 1**	**Level 2**	**Level 3**	**Level 4**	**Sum of Squares**	**Variance**	**F**	**Content of Contribution (%)**
A- Matrıx Type	3	34.87	30.84	41.86	38.00	262.44	87.48	84.77	73.68
B- Fiber volume fraction %	3	32.83	35.81	37.73	39.20	90.67	30.22	29.29	25.45
Error	8					8.26	1.03		0.87
Total	14					361.36	118.73		
For Three-Point Bend Test **S/N ratio: 35.07**		**Average S/N Values**							
	Degrees of Freedom	**Level 1**	**Level 2**	**Level 3**	**Level 4**	**Sum of Squares**	**Variance**	**F**	**Content of Contribution (%)**
A- Matrıx Type	3	32.64	29.86	39.34	38.44	250.54	83.51	346.5	91.56
B- Fiber volume fraction %	3	33.45	34.56	35.67	36.60	22.38	7.46	30.94	8.18
Error	8					1.93	0.24		0.26
Total	14					274.84	91.21		
For Drop Weight Test **S/N ratio: 59.97**		**Average S/N Values**							
	Degrees of Freedom	**Level 1**	**Level 2**	**Level 3**	**Level 4**	**Sum of Squares**	**Variance**	**F**	**Content of Contribution (%)**
A- Matrıx Type	3	57.68	59.76	63.06	59.36	60.84	20.28	25.47	58.62
B- Fiber volume fraction %	3	57.72	59.66	60.33	62.17	40.56	13.52	16.98	39.08
Error	8					6.37	0.80		2.30
Total	14					107.77	34.60		
Hardness Test **S/N ratio: 36.44**		**Average S/N Values**							
	Degrees of Freedom	**Level 1**	**Level 2**	**Level 3**	**Level 4**	**Sum of Squares**	**Variance**	**F**	**Content of Contribution (%)**
A- Matrıx Type	3	36.80	35.03	37.27	36.66	11.41	3.80	73.58	80.25
B- Fiber volume fraction %	3	35.75	36.55	36.68	36.78	2.65	0.88	17.11	18.66
Error	8					0.41	0.05		1.09
Total	14					14.48	4.74		

3.5. Analysis of experimental results

Table 5 shows the test results' signal/noise (S/N) ratios.

After determining the S/N values, the effect of each parameter on the output needs to be analyzed. Therefore, the average of the S/N ratios specified in Table 4 was calculated separately for each level of each parameter. The best experimental result gives the highest S/N ratio. It is shown graphically in Figure 10.

When the S/N ratios of all tests were examined, the mechanical properties of the composites increased as the fiber content increased. It has been observed, however, that the effect of fiber is reduced. This effect can be explained as follows: The recudtion is due to the increase in the deformation energy of the composite with the increase of the fiber fraction and the weakening of the bond strength between the matrix and the fiber. Considering the matrix parameters, the highest effect was observed in the composites made with PA6. However, this is mainly because PA6 has the highest level of mechanical properties among the matrices [53].

ANOVA analysis was performed to understand at what level the independent variables affected the

Table 7. Regression equations for predicting the mechanical properties of composites

Property	Regression Conditions W (Fiber volume fraction)	P (Strength parameter)	Regression Equation
Tensile	W1=1, W2=2, W3=3, W4=4	P1=19, P2=38, P3=85, P4=60	$y(W,P) = 1.129898 \cdot W^{0.5408653} \cdot P^{0.9532715}$
Three-point bending	W1=1, W2=2, W3=3, W4=4	P1=32, P2=27, P3=81, P4=70	$y(W,P) = 1.408406 \cdot W^{0.2568704} \cdot P^{0.9089538}$
Drop weight	W1=1, W2=2, W3=3, W4=4	P1=580.46, P2=672.48, P3=1189.23, P4=752.70	$y(W,P) = 4.797744 \cdot W^{0.3307587} \cdot P^{0.7647516}$
Hardness	W1=1, W2=2, W3=3, W4=4	P1=65, P2=50, P3=70, P4=62	$y(W,P) = 2.814354 \cdot W^{0.0798804} \cdot P^{0.7526531}$

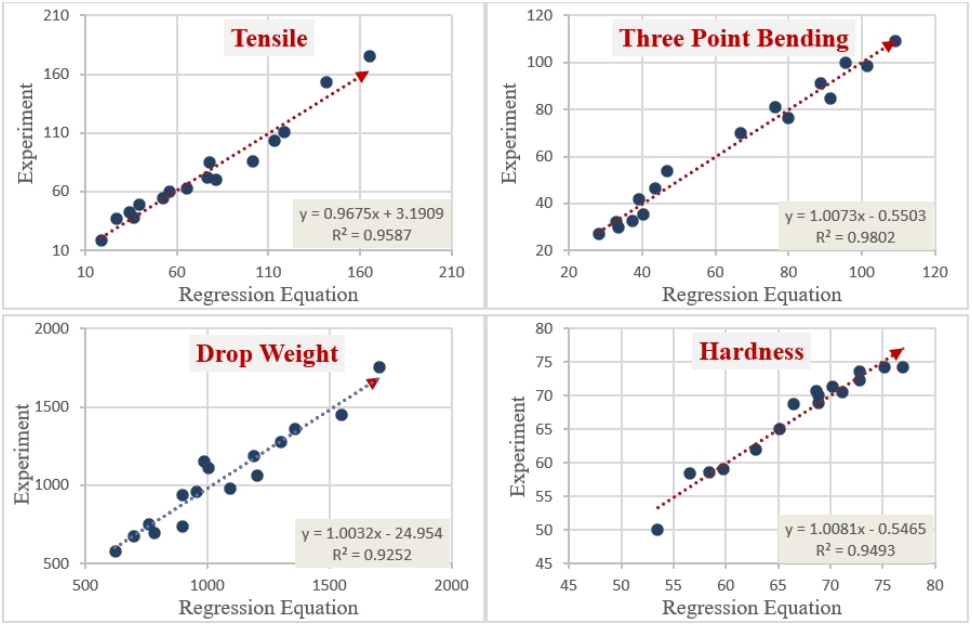

Fig. 11. Scatter diagrams for assessing the generated regression equations for mechanical properties of composites

experimental outcomes. It is shown in detail in Table 6. The calculated F-values were compared with the F0.05;3;8 (4.06) value specified in the F-critical distribution (0.05) table. When we look at the F values we calculated, it is seen that it provides a 95% confidence level [54].

3.6. Regression analysis

This section has developed regression equations to measure the relationship between input and output parameters. The equation constants are obtained by the nonlinear multivariable optimization method. In the equations, the fiber volume fraction (W) and strength parameter (P) were measured for the pure polymer without the addition of fiber, and these values were defined as independent variables ($y(W,P)$, which equal the mechanical properties of the composites. The general representation of the proposed regression equation is shown as follows:

Nonlinear equation (NLE):

$$y(W,P) = \alpha_0 \cdot W^{\alpha_1} \cdot P^{\alpha_2} \tag{6}$$

where y is the equation predicted outcomes and α_0, α_1, α_2 are the equation coefficients (determined by the data-fitting process) [55]. The equation constants above are found by performing regression

analysis, which is shown in Table 6, for mechanical properties of tensile, three-point bending, drop weight, and hardness. In the study of the equations, W and P are both considered as 4 levels [23]. For W, the levels are described as W1 = 1 (0 vol% AF), W2 = 2 (10 vol% AF), W3 = 3 (20 vol% AF), and W4 = 4 (30 vol% AF). On the other hand, the various types of matrix used in this study are assigned at different levels to obtain more accurate equations for the mechanical properties of the composites (Table 7).

The comparative assessments' results between the experimental and model predicted values are shown in Figure 11. The assessment is performed for tensile, three-point bending, drop weight, and hardness by taking into account the error between the experimental values and the regression equation model predicted values. The predicted error percentage between predicted and measured output values at the same W and P values is calculated.

The regression coefficient (R) for the applicability of the model to the mechanical properties of composites was found to be higher than 0.95. The regression coefficient (R) for the applicability of the model to the mechanical properties of composites was found to be higher than 0.95. The error rate was at most 8%. These values are acceptable as the combined parameters are used together [52–56].

These results show that the estimations of the regression models obtained (although they have a nonlinear structure) against the experimental values are very close and at acceptable levels [56]. These errors are due to the smallness of the experimental data set and also because too many parameters were evaluated together. An equation has been established by combining very different factors with the variable parameters of the fiber and matrix type and their contribution rates. Therefore, these errors can be tolerated [57].

4. Conclusions

Our study reinforced short aramid fibers in PP, PE, PA6, and PA12 matrices. The mechanical performance of the composites was affected by the content of aramid fiber, matrix-fiber-interfacial adhesion performance, matrix type, fiber/matrix volume ratio, and homogeneous distribution of fiber in the matrix.

Figure 3 shows that the fiber yield decreases at the transition from 20% to 30% in PA6, and there is a decreasing increase in PA12 at the transition from 20% to 30%. The fiber efficiency decreased as the fiber content increased in the matrix/fiber fraction. The main reason is local deformations in the fibers due to fiber-fiber interaction.

Aramid fiber showed the highest effect on the PE and PP matrices in all tests. This result is related to the PE and PP matrices having lower surface energy than the other matrices.

As shown in Figure 3, the most optimal volume percent ratio of aramid fiber according to the matrices was also investigated. It was found to be 10% by volume for PP, 10% by volume for PE, 20% by volume for PA6, and 30% by volume for PA12. After these values, the fiber yield in the composite tends to decrease. AF was generally found to strengthen the polymers tested well.

Looking at the ANOVA analysis results; The matrix type affected the composites by 74% in the tensile test, 92% in the three-point bending test, 59% in the drop weight test, and 80% in the hardness test; and it was found to be the most influential parameter.

Finally, a nonlinear regression equation related to the experimental results was developed. Looking at the error results, it was seen that the accuracy rate was above 90%, and it was concluded that it was good enough to be correlated with the experimental results of aramid-fiber-reinforced polymer composites.

References

[1] Zhandarov S, Mäder E. Characterization of fiber/matrix interface strength: Applicability of different tests, approaches and parameters. *Compos Sci Technol.* 2005;65: 149–160.

[2] Al-Furjan MSH, Shan L, Shen X, et al. A review on fabrication techniques and tensile properties of glass, carbon, and kevlar fiber reinforced polymer composites. *J Mater Res Technol.* 2022;19: 2930–2959.

[3] Sajan S, Philip Selvaraj D. A review on polymer matrix composite materials and their applications. *Mater Today Proc.* 2021;47: 5493–5498.

[4] Wang M, Pan Z, Wu Z, et al. Effect of carbon/Kevlar asymmetric hybridization ratio on the low-velocity im-

pact response of plain woven laminates. *Compos Struct.* 2021;276: 114574.

[5] Kalantar J, Drzal LT. The bonding mechanism of aramid fibres to epoxy matrices - Part 1 A review of the literature. *J Mater Sci.* 1990;25: 4186–4193.

[6] Muthalagu R, Murugesan J, Sathees Kumar S, et al. Tensile attributes and material analysis of kevlar and date palm fibers reinforced epoxy composites for automotive bumper applications. *Mater Today Proc.* 2021;46: 433–438.

[7] Jaiswal G, Singha MK, Das D. Mechanical behavior of aramid-polypropylene fiberweb composites. *Compos Struct* 2021; 268: 113938.

[8] Amran M, Fediuk R, Vatin N, et al. Fibre-reinforced foamed concretes: A review. *Materials (Basel)* 2020; 13: 1–36.

[9] Geo J, Yang X, Guo J, et al. Hyperelastic mechanical properties of chopped aramid fiber-reinforced rubber composite under finite strain. *Compos Struct* 2020; 243: 112187.

[10] Arroyo M, Bell M. Morphology/behavior relationship and recyclability of composites based on PP/EPDM blends and short aramid fibers. *J Appl Polym Sci.* 2002;83: 2474–2484.

[11] Sarasini F, Tirillò J, Valente M, et al. Hybrid composites based on aramid and basalt woven fabrics: Impact damage modes and residual flexural properties. *Mater Des.* 2013;49: 290–302.

[12] Shibulal GS and Naskar K, Structurally Different Short Aramid Fiber–Reinforced Thermoplastic Polyurethane. *Polymer Composıtes*, 2014; 35(9): 1767-1778. https://doi.org/10.1002/pc.22830

[13] Ari A, Karahan M, Ahmed HAM, Babiker O, Dehşet RMA. A Review of Cellulosic Natural Fibers' Properties and Their Suitability as Reinforcing Materials for Composite Panels and Applications. AATCC Journal of Research. 2023;10(3):163-183. doi:10.1177/24723444221147365

[14] Bazan P, Nosal P, Wierzbicka-Miernik A, et al. A novel hybrid composites based on biopolyamide 10.10 with basalt/aramid fibers: Mechanical and thermal investigation. *Compos Part B Eng*. 223. Epub ahead of print 2021. DOI: 10.1016/j.compositesb.2021.109125.

[15] Vajrasthira C, Amornsakchai T, Bualek-Limcharoen S. Fiber-matrix interactions in aramid-short-fiber-reinforced thermoplastic polyurethane composites. *J Appl Polym Sci.* 2002;87: 1059–1067.

[16] Siva R, Sundar Reddy Nemali S, Kishore Kunchapu S, et al. Comparison of mechanical properties and water absorption test on injection molding and extrusion - injection molding thermoplastic hemp fiber composite. *Mater Today Proc.* 2021;47: 4382–4386.

[17] Crabtree SL, Spalding MA, Pavlicek CL. Single-screw extruder zone temperature selection for optimized performance. *Tech Pap Reg Tech Conf - Soc Plast Eng.* 2008;3: 1406–1411.

[18] da Costa HM, Ramos VD, de Oliveira MG. Degradation of polypropylene (PP) during multiple extrusions: thermal analysis, mechanical properties and analysis of variance. *Polym Test.* 2007;26: 676–684.

[19] Fu SY, Lauke B, Mäder E, et al. Tensile properties of short-glass-fiber- and short-carbon-fiber-reinforced polypropylene composites. *Compos Part A Appl Sci Manuf.* 2000;31: 1117–1125.

[20] Delli E, Giliopoulos D, Bikiaris DN, et al. Fibre length and loading impact on the properties of glass fibre reinforced polypropylene random composites. *Compos Struct*. 263. Epub ahead of print 2021. DOI: 10.1016/j.compstruct.2021.113678.

[21] Savaşkan M, Taptık Y, Ürgen M. Deney tasarımı yöntemi ile matkap uçlarında performans optimizasyonu. *Itüdergisi/D.* 2004;117–128.

[22] Kumar S, Balachander S. Studying the effect of reinforcement parameters on the mechanical properties of natural fibre-woven composites by Taguchi method. *J Ind Text.* 2020;50: 133–148.

[23] Özçelik B, Özbay B. Plastik Enjeksiyon Kalıp Malzemelerinin Polipropilen Ürünün Mekanik Özeliklerine Etkisinin Taguchi Yöntemiyle Belirlenmesi. *Sigma 29.* 2011;289–300.

[24] Fu T, Haworth B, Mascia L. Analysis of process parameters related to the single-screw extrusion of recycled polypropylene blends by using design of experiments. *J Plast Film Sheeting.* 2017;33: 168–190.

[25] Ravi Kumar N, Srikant P, Ranga Rao CH, et al. Statistical analysis of mechanical properties of vakka fiber reinforced polypropylene composites using Taguchi method. *Mater Today Proc.* 2017;4: 3361–3370.

[26] Li T, Wang Z, Zhang H, et al. Non-destructive modification of aramid fiber by building nanoscale-coating solution to enhance the interfacial adhesion properties of the fiber-reinforced composites. *J Compos Mater.* 2021;55: 1823–1834.

[27] Zhang B, Jia L, Tian M, et al. Surface and interface modification of aramid fiber and its reinforcement for polymer composites: a review. *Eur Polym J.* 2021;147: 110352.

[28] Huang BZ, Zhao LJ. Bridging and toughening of short fibers in SMC and parametric optimum. *Compos Part B Eng.* 2012;43: 3146–3152.

[29] Wang J, Fuentes CA, Zhang D, et al. Wettability of carbon fibres at micro- and mesoscales. *Carbon N Y.* 2017; 120: 438–446.

[30] Lu C, Wang J, Lu X, et al. Wettability and interfacial properties of carbon fiber and Ppoly(ether ether ketone) fiber hybrid composite. *ACS Appl Mater Interfaces.* 2019;11: 31520–31531.

[31] Carroy A, Druene L, Garinet M, et al. Hooked on plastics - How to get your UV coating to adhere. *Paint Coatings Ind.* 2006;22: 46–52.

[32] Surface treatments improve adhesion to composites | 2017-09-21 | *Assembly Magazine* | ASSEMBLY [Internet]. [cited 2023 Mar 16]. https://www.assemblymag.com/articles/93987-surface

-treatments-improve-adhesion-to-composites
[33] Surface energy of plastics, https://www.tstar.com/blog/bid/33845/surface-energy-of-plastics [Accessed 16 March 2023].
[34] Technology: Silicone Adhesion & Bonding — News — Compo-SiL®, https://www.compo-sil.com/modules/news/article.php?storyid=57 [Accessed 16 March 2023].
[35] PP Bonding|PTFE Gluing|HDPE|LDPE bond|Polypropylene joining, https://elixir-india.net/blog/polyeolefin-bonding/ [Accessed 16 March 2023].
[36] Şekercioğlu T, Üniversitesi P, Fakültesi M, et al. Investigation of Surface Preparation Methods for Bonding of PlasticPlastiklerin Yapiştirilmasinda Yüzey HazirlamYöntemleriniİncelenmesi. 2014;37–44.
[37] Biswas ma K, Shayed ma, Hund rd, et al. Surface modification of Twaron aramid fiber by the atmospheric air plasma technique. *Text Res J.* 2013; 83: 406–417.
[38] Yuan H, Wang W, Yang D, et al. Hydrophilicity modification of aramid fiber using a linear shape plasma excited by nanosecond pulse. *Surf Coatings Technol.* 2018;344: 614–620.
[39] Karahan M, Karahan N. Influence of weaving structure and hybridization on the tensile properties of woven carbon-epoxy composites. *J Reinf Plast Compos.* 2014;33: 212–222.
[40] Wang C, Li KZ, Li HJ, et al. Effect of carbon fiber dispersion on the mechanical properties of carbon fiber-reinforced cement-based composites. *Mater Sci Eng A.* 2008;487: 52–57.
[41] Bingöl M, Çavdar K. Effects of different reinforcements for improving mechanical properties of composite materials. *Uludağ Univ J Fac Eng.* 2016;21: 123.
[42] Wang Y, Hansen CJ, Wu CC, et al. Effect of surface wettability on the interfacial adhesion of a thermosetting elastomer on glass. *RSC Adv.* 2021;11: 31142–31151.
[43] Ari A, Bayram A, Karahan M, et al. Comparison of the mechanical properties of chopped glass, carbon, and aramid fiber reinforced polypropylene. *Polym Polym Compos.* 2022;30: 096739112210985. https://doi.org/10.1177/09673911221098570
[44] Karahan M, Gul H, Karahan N, et al. Static behavior of three-dimensional Integrated core sandwich composites subjected to three-point bending. *J Reinf Plast Compos.* 2013;32: 664–678.
[45] Laura DM, Keskkula H, Barlow JW, et al. Effect of glass fiber and maleated ethylene-propylene rubber content on tensile and impact properties of Nylon 6. *Polymer (Guildf).* 2000;41: 7165–7174.
[46] Guo Q, Xiao B, Ohsawa I, et al. Fracture mechanism characteristics of ultra-thin chopped carbon fiber tape-reinforced thermoplastics hat-shaped hollow beam under transverse static and impact loadings. *Carbon Lett.* 2020;30: 271–280.
[47] Dorigato A, Fambri L. Effect of aramid regenerated fibers on thermo-mechanical behaviour of polyamide 12 composites. *J Reinf Plast Compos.* 2013;32: 1243–1256.
[48] Karahan M, Karahan N. Effect of weaving structure and hybridization on the low-velocity impact behavior of woven carbon-epoxy composites. *Fibres Text East Eur.* 2014;105: 109–115.
[49] Suresha B, Ravi Kumar BN, Venkataramareddy M, et al. Role of micro/nano fillers on mechanical and tribological properties of polyamide66/polypropylene composites. *Mater Des.* 2010;31: 1993–2000.
[50] Abasi FO, Aabass RU. Thermo-mechanical behavior of epoxy composite reinforced by carbon and Kevlar fiber. *MATEC Web Conf.* 2018;225: 1–8.
[51] Andó M, Kalácska G, Czigány T. Shore D Hardness of Cast PA6 Based Composites. 2009;XXIII: 15–19.
[52] Hu C, Liao X, Qin QH, et al. The fabrication and characterization of high density polyethylene composites reinforced by carbon nanotube coated carbon fibers. *Compos Part A Appl Sci Manuf.* 2019;121: 149–156.
[53] Arı A, Bayram A. High-pressure resistant aramid fiber reinforced polymer matrix composite pipe design. Hacettepe Journal of Biology and Chemistry. 2022; 50(3): 301-312. https://doi.org/10.15671/hjbc.1024810
[54] Somashekhar S, Shanthakumar GC, Nagamadhu M. Influence of fiber content and screw speed on the mechanical characterization of jute fiber reinforced polypropylene composite using Taguchi method. *Mater Today Proc.* 2019;24: 2366–2374.
[55] Manikandan A, Rajkumar R. Evaluation of mechanical properties of synthetic fiber reinforced polymer composites by mixture design analysis. *Polym Polym Compos.* 2016;24: 455–462.
[56] Junaedi H, Baig M, Dawood A, et al. Modeling analysis of the tensile strength of polypropylene base short carbon fiber reinforced composites. *J Mater Res Technol.* 2021;11: 1611–1621.
[57] Ari A, Bayram A, Karahan M, et al. Evaluation of the mechanical properties of chopped carbon fibre reinforced polypropylene, polyethylene, polyamide 6, and polyamide 12 composites, In: Industria Textila, 2023; 74(2): 175–183. http://doi.org/10.35530/IT.074.02.202214

Received 2023-01-13
Accepted 2023-05-05